Available online at www.sciencedirect.com

ScienceDirect

Energy Procedia 49 (2014) 447 – 456

Energy Procedia

SolarPACES 2013

High-temperature fluidized receiver for concentrated solar radiation by a beam-down reflector system

K. Matsubara[a,] *, Y. Kazuma[a], A. Sakurai[a], S. Suzuki[a], L. Soon-Jae[a]
T. Kodama[a], N. Gokon[a], C. Hyun Seok[a] and K. Yoshida[a,b]

[a]*Niigata University, 8050 Ikarashi 2-nocho, Nishiku, Niigata 950-2181, Japan*
[b]*The Institute of Applied Energy,14-2 Nishi-Shimbashi 1-Chome, Minato-ku, Tokyo 105-0003, Japan*

Abstract

This study proposes a novel fluidized receiver for absorbing concentrated solar light at high temperatures. Previously, a tubular receiver and a volumetric receiver were developed to make high-temperature air for a solar gas turbine system. The aim was to combine these elements with a tower reflector; however, it was challenging to install these heavy receivers on the top of the tower. Currently, a fluidized receiver prototype is tested by a 3 kWh solar simulator in preparation for a field test at the Miyazaki beam-down reflector system. The fluid dynamics of the prototype receiver is numerically investigated. The currently treated receiver is an inner-circulating fluidized bed spouted by concentric gas streams with high and low velocities in the center and outer annulus, respectively. The draft tube is submerged in the particles to organize particle circulation. Concentrated light irradiates the particles through a quartz window at the top of the receiver container. Such a fluidized bed was first adopted by Kodama et al. for thermochemical reactions; however, it is currently pursued for its potential as a high-temperature receiver aimed at concentrated solar power generation. Experiments of the prototype receiver (inner diameter = 45 mm) demonstrated that the inner particles are heated to a temperature greater than 900°C and that an increase of the central gas velocity removes the excess temperature near the particle bed surface. A numerical computation suggests that the large-scale circulation of particles leads to the activation of thermal mixing. The currently proposed receiver is thus expected to attenuate re-radiation losses likely to occur in a conventional volumetric porous receiver. The scale-up of the receiver is being considered by the numerical computation for a field test in the Miyazaki 100 kWh beam-down reflector system.

Selection and peer review by the scientific conference committee of SolarPACES 2013 under responsibility of PSE AG.
Final manuscript published as received without editorial corrections.

* Corresponding author. Tel.:+81-(0)25-262-7260;fax:+81-(0)25-262-7260.
E-mail address: matsu@eng.niigata-u.ac.jp

Selection and peer review by the scientific conference committee of SolarPACES 2013 under responsibility of PSE AG.
Final manuscript published as received without editorial corrections.
doi:10.1016/j.egypro.2014.03.048

Keywords: Solar receiver; Fluidized bed; Numerical simulation; Solar simulator; Beam-down reflector system

1. Introduction

Concentrated solar power (CSP) has been practically applied in European countries and the United States. New CSP plants are planned to be built in the Middle East and North Africa, China, and India. Recent CSP systems adopt tower-type point concentration (see Fig. 1(a)). Such systems use a molten nitrate salt for heat transport and as heat storage media for power generation by means of a steam turbine engine. Currently, the temperatures of heat transport and heat storage are as high as 560°C [1]. However, solar concentration at higher temperatures is required for improvements in the CSP system. If the heat source is increased to greater than 900°C, a hot air turbine can be installed to enhance the energy output. The use of a hot air turbine promises to better accommodate CSP in desert areas where cooling water is scarce. The extension of a hot air turbine to a combined cycle is expected to increase the thermal efficiency to higher than 50%, as estimated from similar improvements to conventional power plants.

Efforts are being made for air receiver research and development to overcome the weakness associated with the use of nitrate salts, which pyrolytically decompose at temperatures greater than 600°C [2]. The Deutsches Zentrum für Luft- und Raumfahrt (DLR; German Aerospace Center) developed a volumetric receiver, which consists of a quartz window and SiC foam directly irradiated by solar light [2]. They also developed a tubular receiver, cup-shaped structure. These receivers are designed to be installed on the top of the CSP tower. However, it is challenging to place heavy receivers at a height greater than 100 m, which deters the implementation of the developed system in a working plant. Another problem exists regarding the operation of the heat storage system at high temperatures. The DLR is studying the use of a particle receiver to accumulate the heated particles as a thermal medium [2]. Sandia National Laboratory is testing the use of a falling-sand receiver [3].

This study describes a new concept of an air receiver that utilizes an inner-circulating fluidized bed for high-temperature thermal concentration from condensed solar light. This fluidized receiver is suitable for extension to a heat storage system, since the heated particles can be streamed for storage. This study focuses on the characteristics of thermal concentration by the irradiated particles as the first step. The currently discussed new solar receiver is planned to be combined with the beam-down solar reflector system (see Fig. 1(b)) built on the campus of the University of Miyazaki. To prepare for the field test, the receiver prototype was tested using a 3 kWh solar simulator to measure the temperature distribution of particles and the thermal output of the exhaust gas. The flow fields of the fluidized particles are numerically computed by a granular model. The velocity vectors of solid particles are discussed to reveal the flow structures and heat transport mechanisms. This study also treats a volumetric receiver composed of a porous ceramic, since characteristics of this receiver can be used as a reference for the newly developed particle receiver acting with no fluidization.

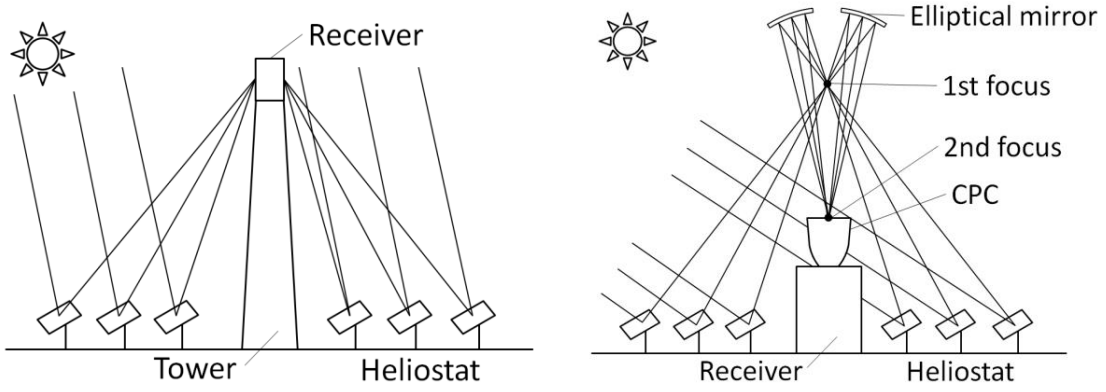

(a) Conventional tower system, (b) Beam-down reflector system.

Fig. 1. Schematics of CSP reflector systems.

Nomenclature

c_f	*fluid specific heat*
d_p	particle diameter
D_B	inner diameter or width of receiver
D_P	width of porous medium
D_T	inner diameter of draft tube
F	inertia coefficient of porous media
$\vec{F}_s$	external force vector for solid phase
h_v	volumetric heat transfer coefficient
h_{sf}	heat transfer coefficient between fluid and porous matrix
H_B	height of non-fluidized bed
H_P	height of porous medium
H_T	height of draft tube
k	permeability
$\dot{m}_{fs}$	mass transfer rate between fluid and solid
p	pressure
$\vec{R}_{fs}$	phase interaction vector
T_f	fluid temperature
T_s	solid temperature
u	fluid horizontal velocity
$\vec{u}_{fs}$	slip velocity vector of solid phase
u_s	solid-phase horizontal velocity
$\vec{u}_s$	velocity vector of solid phase
v	fluid vertical velocity
v_s	solid-phase vertical velocity
V_D	inlet velocity of gas at central part
V_A	inlet velocity of gas at annuli
x	coordinate in lateral direction
y	coordinate in vertical direction
α_s	volume rate of solid phase
α_{sf}	specific surface per unit volume
γ_s	dissipation rate of granular phase
δ_T	thickness of draft tube
ε	porosity
θ_s	granular-phase temperature
$\kappa_{\theta s}$	diffusion coefficient in granular-phase temperature equation
$\lambda_{f,eff}$	effective thermal conductivity of fluid
λ_s	thermal conductivity of solid
$\lambda_{s,eff}$	effective thermal conductivity of solid
μ_f	fluid viscosity
μ_{eff}	effective fluid viscosity
ρ_f	fluid density
$\bar{\bar{\tau}}_s$	solid stress tensor
ϕ_{lm}	exchange term in granular-phase temperature equation
ϕ_{fs}	exchange term in granular-phase temperature equation

2. Numerical computation of the volumetric receiver

Numerical computations of the volumetric air receiver are described before the discussion of the fluidized receiver. The computational domain for this receiver is presented in Fig. 2. As described in the figure, the receiver is composed of a porous medium and a container with a quartz glass cover, irradiated by concentrated light. The air stream at room temperature is suctioned into the container, heated by the irradiated porous medium, and is exhausted from the bottom exit. The numerical scheme follows the two-equation approach by Xu et al. [4]. This study uses the basic equations [3]:

$$\frac{\partial(\rho_f u)}{\partial x}+\frac{\partial(\rho_f v)}{\partial y}=0 \tag{1}$$

$$\frac{\rho_f}{\varepsilon}\left(u\frac{\partial u}{\partial x}+v\frac{\partial u}{\partial y}\right)=-\frac{\partial p}{\partial x}+\mu_{eff}\left(\frac{\partial^2 u}{\partial x^2}+\frac{\partial^2 u}{\partial y^2}\right)-\left(\frac{\mu_f}{k}+\frac{\rho_f F\varepsilon}{\sqrt{k}}u\right)u \tag{2}$$

$$\frac{\rho_f}{\varepsilon}\left(u\frac{\partial v}{\partial x}+v\frac{\partial v}{\partial y}\right)=-\frac{\partial p}{\partial y}+\mu_{eff}\left(\frac{\partial^2 v}{\partial x^2}+\frac{\partial^2 v}{\partial y^2}\right)-\left(\frac{\mu_f}{k}+\frac{\rho_f F\varepsilon}{\sqrt{k}}v\right)v \tag{3}$$

$$\frac{\partial(\rho_f c_f u T_f)}{\partial x}+\frac{\partial(\rho_f c_f v T_f)}{\partial y}=\lambda_{f,eff}\left(\frac{\partial^2 T_f}{\partial x^2}+\frac{\partial^2 T_f}{\partial y^2}\right)+h_v(T_s-T_f) \tag{4}$$

$$\lambda_{s,eff}\left(\frac{\partial^2 T_s}{\partial x^2}+\frac{\partial^2 T_s}{\partial y^2}\right)-h_v(T_s-T_f)=0 \tag{5}$$

The effective viscosity, μ_{eff}, the permeability, k, and the inertia coefficient of porous media, F, are calculated from

$$\mu_{eff}=\frac{\mu_f}{\varepsilon} \tag{6}$$

$$k=\frac{d_p^2\varepsilon^3}{150(1-\varepsilon)^2} \tag{7}$$

$$F=\frac{1.75}{\sqrt{150}\varepsilon^{3/2}} \tag{8}$$

where ε is the porosity, and d_p is the diameter of particles. The volumetric heat transfer coefficient, h_v, is calculated by

$$h_v=h_{sf}\alpha_{sf}, \tag{9}$$

where h_{sf} is the heat transfer coefficient between the fluid and the porous matrix, and α_{sf} is the specific surface area per unit volume. This study uses the heat transfer models by Hwang et al. [5] and Alazami and Vafai [6] for h_{sf} and α_{sf}.

The basic equations are solved by the SIMPLE method by S.V. Patankar [7]. The upwind finite difference is used for the convection terms, whereas the central difference is used for the diffusion terms. Figure 3 exemplifies the temperature distribution computed for the prescribed numerical condition: the width of the porous medium D_P = 200 mm, the thickness of the medium H_P = 20 mm, the particle diameter d_p = 0.1 mm, and the porosity $\varepsilon = 0.25$.

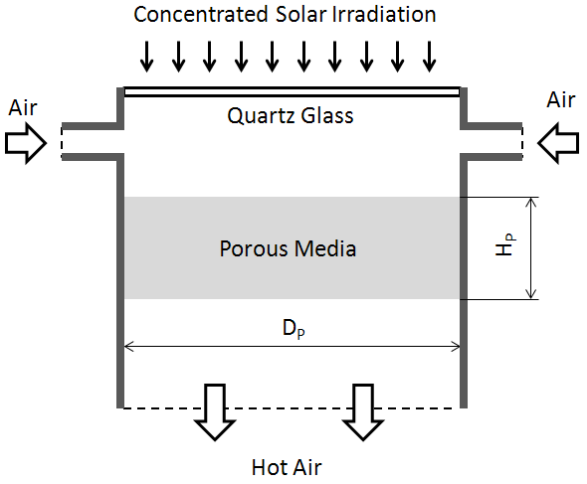

Fig. 2. Schematic of the computational domain of the volumetric receiver.

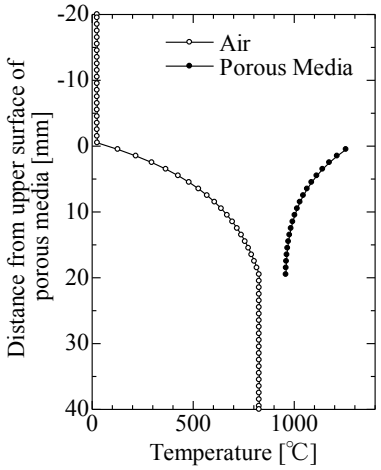

Fig. 3. Temperature distribution in the volumetric air receiver.

The thermal properties of SiC are assumed as λ_s = 118 W/(mK). The inlet air velocity is prescribed so that the velocity normal to the surface of the porous medium is equal to 0.05 m/s. The irradiation of concentrated light is treated as heat generation at the porous surface of 1,000 kW/m^2.

The temperature distribution of the air and the porous medium along the center line is presented in Fig. 3. According to the figure, the porous medium emits hot air at temperatures greater than 800°C. The temperature of the porous medium increases to greater than 1300°C on its top surface and transports heat to the air to be cooled to 1000°C at the bottom surface. There is wide thermal scattering between the temperatures of the air and the porous medium at the top surface. Since re-radiation of heat is proportional to the absolute temperature with power of four, the excess temperature on the porous surface is likely to trigger energy loss by re-radiation. With respect to flow characteristics, the pressure loss penalty is evaluated to be 0.786 MPa by the simulation. This value is higher than that of the fluidized receiver, since the particle size is much smaller than that of the fluidized receiver. The current temperature distribution of solid differs from the existing paper where the solid temperature increases from the porous surface. The thermal boundary condition on the porous surface needs to be elaborated to improve numerical credibility.

3. Experimental examination of the fluidized receiver

Figure 4 shows photographs of the experimental setup [8]. The prototype of the fluidized receiver with the quartz window is tested by a 3 kWh solar simulator in preparation for its demonstration at the Miyazaki 100 kWh beam-down reflector system. The radiation flux is measured by the Gardon gauge to reveal a thermal power of 2.65 kWh irradiated on a 45-mm-diameter aperture. The averaged radiation flux is 1670 kW/m^2. The concept of the receiver is illustrated in Fig. 5. The height of the particle bed, H_B, in Fig. 5 is defined as the non-fluidized bed height. Non-reactive particles are poured into the receiver column, being fluidized by the air streams from the distributing plates of the stainless steel mesh at the bottom. The inner diameter of the receiver column is D_B= 45 mm. Concentrated light irradiates the surface of the particle bed through the quartz window at the top. The air at the central distributor flows faster than the surrounding air from the annuli, which substantiates the incitement of organized particle circulation demonstrated by numerical computations. The draft tube is submerged in the fluidized bed to stabilize this circulation.

The inner diameter of the draft tube is D_T= 20 mm, its thickness is δ_T= 2 mm, and its height is H_T= 12 mm. In the experiment, the gas velocity, V_D, at the center is increased in stages such that V_D= 3.5 m/s, 5.3 m/s, and 8.8 m/s, maintaining the ratio between the central and annular velocities, V_D/V_A, at a constant value of 1.56. The

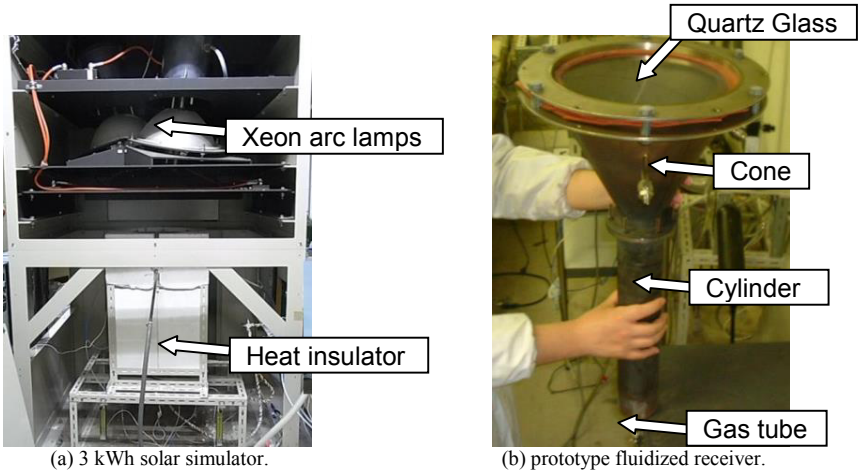

(a) 3 kWh solar simulator. (b) prototype fluidized receiver.

Fig. 4. Experimental setup.

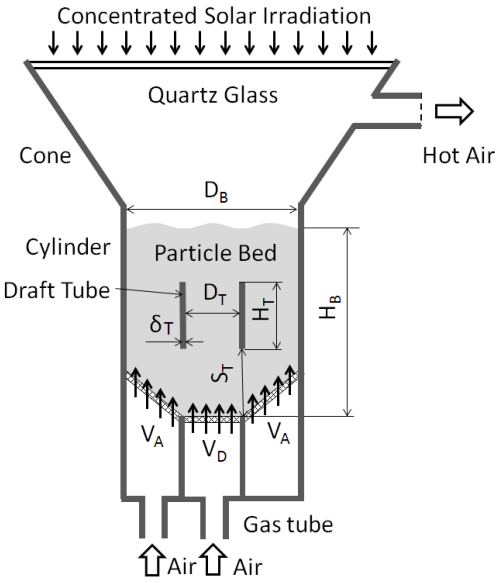

Fig. 5. Schematic of the fluidized-bed receiver.

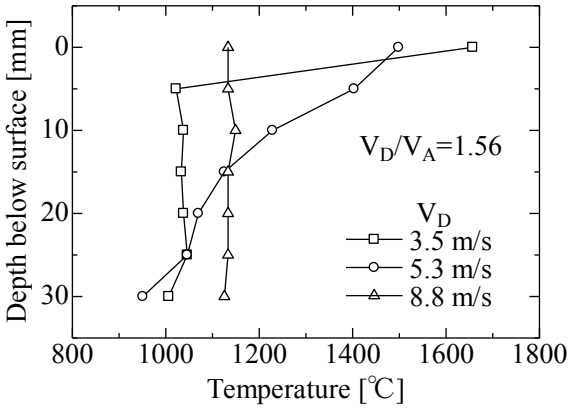

Fig. 6. Temperature distribution in the fluidized-bed receiver.

experimental unit is made using $NiFe_2O_4/mZrO_2$ ceramic particles having a diameter of 212–710 μm.

The temperature distribution along the centerline is shown in Fig. 6. The temperature is measured by an R-type thermocouple. The temperature is different between the solid and air in the fluidized receiver. However, these temperatures cannot be separately measured. This study measures the mean temperature of solid and air at each location. In this experiment, the temperature is high near the particle bed surface when V_D = 3.5 m/s. However, when the central velocity is increased, maintaining the velocity ratio V_D/V_A constant, this excess temperature is attenuated and the temperature distribution is flattened. This suggests that thermal mixing is enhanced by acceleration of the gas streams.

4. Numerical computation of the fluidized receiver

A numerical computation is conducted by FLUENT V. 13 to evaluate the physics of the fluidized bed. The numerical computation is developed for the computational domain depicted in Fig. 7. A two-dimensional simulation is conducted, since a three-dimensional simulation requires enormous computational time. The boundary condition for the inlet velocity is given at the inner surface of the porous distributor for the simplicity of the simulation. The velocity is assumed to be uniformly distributed on the distributor parallel to the cylinder axis. The cone is neglected in the simulation.

A granular approach is adopted to treat the solid–fluid, two-phase flow. The basic equations are given for the granular-phase flow as follows:

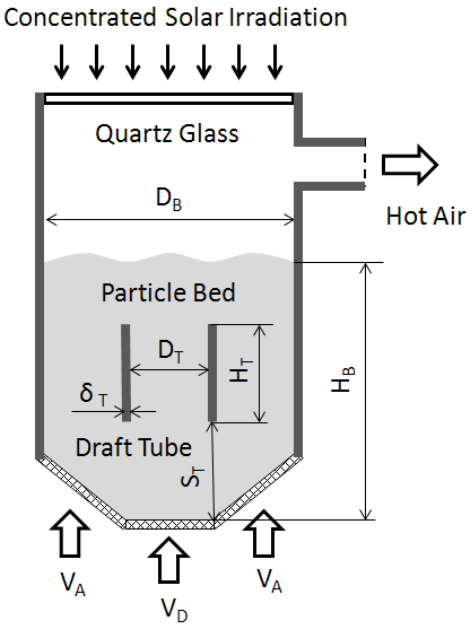

Fig. 7. Computational domain for the fluidized receiver.

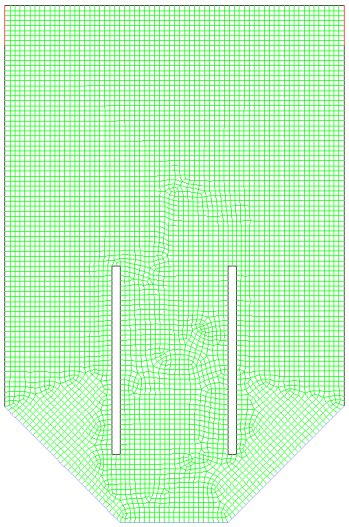

Fig. 8. Arrangement of grid points (for Case 6).

Table 1 Numerical conditions for fluidized receiver simulation.

Case	Inner diameter of the receiver column, D_B, mm	Inner diameter of the draft tube, D_T, mm	Thickness of the draft tube, δ_T, mm	Height of the non-fluidized bed, mm	Gas velocity, V_D, m/s	Gas velocity at the annular part, V_A, m/s	Number of grid points
Case 1	85	47	2	85	0.5	0.1	6530
Case 2	160	68	2	160	0.5	0.1	9158
Case 3	160	-	-	160	0.5	0.1	9277
Case 4	160	68	2	160	1.0	0.2	9158
Case 5	160	68	2	160	0.25	0.05	9158
Case 6	250	106	5	250	0.5	0.1	9103
Case 7	250	-	-	250	0.5	0.1	9186

$$\frac{\partial}{\partial t}\left(\alpha_s \rho_s\right)+\nabla\cdot\left(\alpha_s \rho_s \vec{u}_s\right)=\dot{m}_{fs} \tag{10}$$

$$\frac{\partial}{\partial t}\left(\alpha_s \rho_s u_s\right)+\nabla\cdot\left(\alpha_s \rho_s \vec{u}_s \vec{u}_s\right)=-\alpha_s \nabla p_f+\nabla\cdot\bar{\tau}_s+\sum_{s=1}^{n}\left(\vec{R}_{fs}+\dot{m}_{fs}\vec{u}_{fs}\right)+\vec{F}_s \tag{11}$$

The second term on the right-hand side of equation (11) is the solid stress tensor. The third term in parenthesis on the right-hand side of equation (11) is the phase interaction term. The basic equation for the granular-phase temperature is

$$\frac{3}{2}\left\{\frac{\partial}{\partial t}\left(\alpha_s \rho_s \theta_s\right)+\nabla\cdot\left(\alpha_s \rho_s \vec{u}_s \theta_s\right)\right\}=\bar{\tau}_s : \nabla\vec{u}_s+\nabla\cdot\left(\kappa_{\theta s}\nabla\theta_s\right)-\gamma_s+\varphi_{lm}+\varphi_{fs} \tag{12}$$

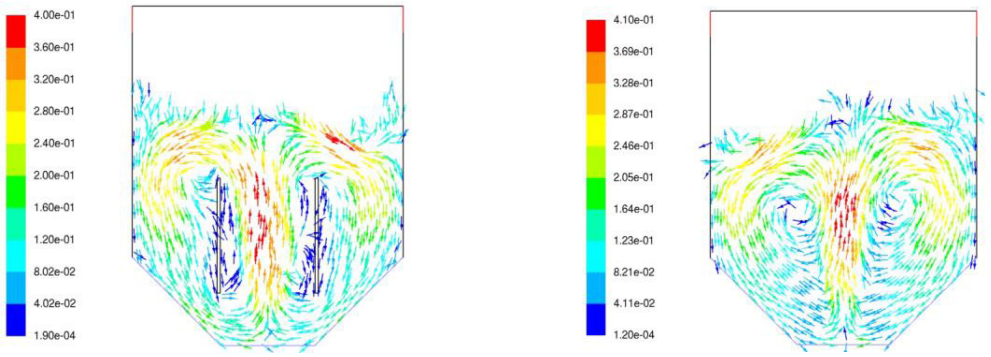

(a) Case 2 (D_B = 160 mm), (b) Case 3 (D_B = 160 mm)

Fig. 9. Velocity vectors of the fluidized particles (Cases 2 and 3).

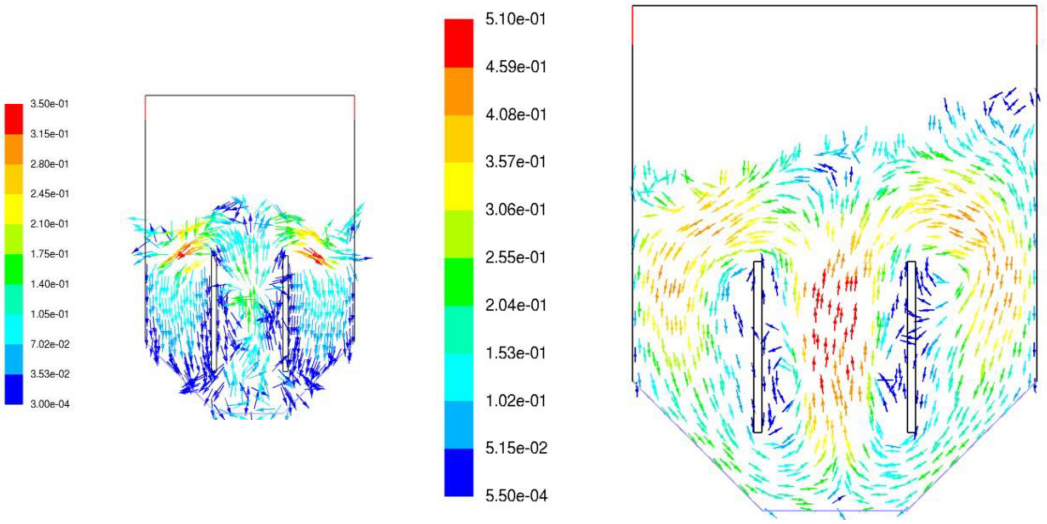

(a) Case 1 (D_B = 85 mm), (b) Case 6 (D_B = 250 mm)

Fig. 10. Velocity vectors of the fluidized particles (Cases 1 and 8).

The first term on the right-hand side is the production term, the second term is the diffusion term, the third is the dissipation term due to inelastic collisions, and the fourth and fifth terms are the exchange terms. The SIMPLE method by Patankar et al. [7] is used to solve these equations. The third-order finite difference method QUICK is applied to the convection terms. The seven numerical conditions listed in Table 1 are numerically computed. Cases 3 and 7 treat the receiver with no draft tube. The input properties of the particles are a density of 5,658 kg/m^3, a specific heat of 635.4 J/kgK, and a thermal conductivity of 2.25 W/mK. Although the particle diameter is not uniform in the experiment, this is set to a constant value of 450 μm in the simulation for simplicity. Figure 8 shows the grid arrangement for Case 6. The number of grid points is listed in Table 1. The numerical grids are doubled in the test simulation for the condition of Case 6. This test simulation also computes the thermal field, and the thermal field significantly depends on the size of the numerical grid. However, the flow field is nearly independent of the numerical grid currently used.

Figures 9 and 10 show the velocity vectors of the fluidized particles. The maximum velocity of the particles is observed to be lower than the inlet gas speed listed in Table 1. According to the numerical results included in these figures, the particles flow inversely in the annular region to circulate globally within the receiver column regardless of the numerical conditions currently treated. The active heat transport observed in the receiver experiment is thus thought to occur because of the enthalpy transport of the particles circulating in the receiver column globally.

The organized flow is compared between cases with a draft tube and those with no draft tube in Fig. 9. Global circulation is commonly observed in both cases. However, the draft tube is confirmed to clearly separate the central up-flow region from the annular down-flow region, and it is consistent for the stabilization of flow circulation. The flow pattern changes little with changing the column diameter from 85 mm to 250 mm when the gas velocity is maintained constant. In the Miyazaki beam-down system, the aperture of the concentrated solar light at the CPC (Compound Parabolic Concentrator) (see Fig. 1) is planned to be 200 to 300 mm. According to the numerical computation, the large size of the receiver column is acceptable for the Miyazaki scale-up demonstration to achieve activated heat transport by particle circulation.

The pressure loss penalty is computed from the numerical computation and is plotted against the particle bed height [mm] in Fig. 11. In the figure, there are no severe effects from the gas velocity and presence of the draft tube. The pressure loss penalty increases according to the particle bed height. Since the current concept of the fluidized receiver keeps the height of the particle bed equal to the inner diameter of the receiver column, high pressure is needed to scale up the receiver for the beam-down reflector system demonstration.

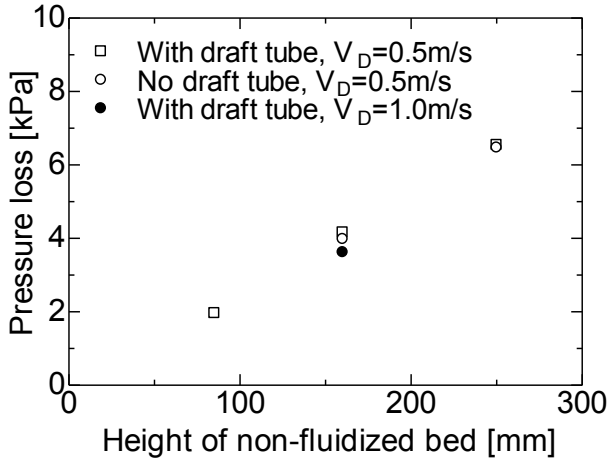

Fig. 11. Pressure losses of the fluidized receiver.

5. Conclusions

This study treats a prototype fluidized receiver for the concentration of solar energy at high temperatures for highly efficient CSP. Experiments using a 3.0 kWh solar simulator and numerical computation are performed for the prototype receiver. Numerical computation is performed for a volumetric receiver to obtain reference data. The conclusions can be summarized as follows.

(1) The volumetric air receiver exhibits excess temperature near the surface of the porous medium due to irradiation by concentrated light. This result derives from low heat transport by means of thermal conductivity of the porous medium in comparison with convective transport. This excess temperature is likely to increase heat release from the material due to thermal radiation, triggering re-radiation losses.

(2) The experimental test of the prototype fluidized receiver demonstrates that particle temperature in the fluidized bed exceeds 900°C from the concentrated radiation of the solar simulator system. When increasing the central velocity, the temperature distribution flattens through the disappearance of the hot spot near the particle bed surface. Therefore, an increase of the central velocity is suggested for the activation of thermal mixing in the particle bed.

(3) Numerical computations by a granular approach indicate that the particles in the fluidized bed demonstrate global circulation in the receiver column. This circulation tends to be aided by the draft tube submerged in the particle bed. The activated heat transport observed in the experiment is thought to occur because of enthalpy transport by the global circulation of the traveling particles. The temperature simulation and the comparison between that and experiment are planned as a next step of the study.

References

[1] SOLGATE Solar Hybrid Gas Turbine Electric Power System, Contract ENK5-CT-2000-00333, Final Publishable Report, 2005.
[2] P. Heller et al., Solar Energy, 2006, 80, 1225.
[3] K. Kim et al., Solar Energy, 2009, 83, 1784.
[4] C. Xu, Z. Song, L. Chen and Y. Zhen, “Numerical investigation on porous media heat transfer in a solar tower receiver,” Renewable Energy, 2011, 36, 1138.
[5] G.J. Hwang, C.C. Wu and C.H.Chao, “Investigation of non-Darcian forced convection in an asymmetrically heated sintered porous channel,” J. Heat Transfer, 1995, 117(8), 725-731.
[6] B. Alazami and K. Vafai, “Analysis of variants within the porous media transport models,” J. Heat Transfer, 2000, 122(5), 303-312.
[7] S. V. Patankar and D.B. Spalding, “A calculation procedure for heat, mass and momentum transfer in three-dimensional parabolic flows,” Int. J. Heat Mass Transfer, 1972, 15(10), 1787-1806.
[8] T. Fend, R.Pitz-Paal, O. Reutter, J. Bauer and B. Hoffschmidt, “Two Novel High-Porosity Materials as Volumetric Receivers For Concentrated Solar Radiation”, Solar Energy Materials & Solar Cells, 2004, 84, 291-304.
[9] N. Gokon, H. Yamamoto, N. Kondo and T. Kodama, “Internally circulating fluidized bed reactor using m-ZrO_2 supported $NiFe_2O_4$ particles for thermochemical two-step water splitting”, ASME J. Solar Engineering, 2010, 132, 021102 (10 Pages)
[10] Gidaspow, D., Jiradilok, V., “Computational Techniques: The Multiphase CFD Approach to Fluidization, and Green Energy Technologies”, Nova Science Pub Inc., 2010.